Electric field gradients of ^{111}Cd in monoclinic (B-phase) rare earth sesquioxides

1994 J. Phys.: Condens. Matter 6 10445

(http://iopscience.iop.org/0953-8984/6/48/006)

J. Phys.: Condens. Matter 6 (1994) 10445–10456. Printed in the UK

Electric field gradients of ^{111}Cd in monoclinic (B-phase) rare earth sesquioxides

Doru Lupascu, Michael Uhrmacher and Klaus Peter Lieb

II. Physikalisches Institut, Universität Göttingen, Bunsenstrasse 7-9, D-37073 Göttingen, Germany

Received 22 July 1994

Abstract. Perturbed γ–γ angular correlation measurements with ^{111}In(EC) ^{111}Cd probes have been performed in the monoclinic (B-phase) rare earth sesquioxides Sm_2O_3, Eu_2O_3 and Gd_2O_3. The spectra in all three oxides show a dominating electric field gradient of high asymmetry, $\eta \approx 1$, and strong coupling constant, $\nu_Q \approx 208$ MHz, at room temperature. A slight modification of the structure in this phase with temperature was observed, but no phase transition occurred. Unlike the other structural isomorphs of the rare earth oxides, the cationic lattice sites in the B phase are not equally occupied by the implanted ^{111}In ions in the temperature range investigated (10–900 K). The point-charge model and symmetry considerations were used to associate the dominating electric field gradient with substitutional ^{111}In on the crystallographic site M(3). Two additional electric field gradients populated in small fractions were found in limited temperature ranges and tentatively attributed to defects.

1. Introduction

The sesquioxides of Gd, Eu and Sm crystallize essentially in two crystal modifications: at low temperatures the cubic C-phase prevails (bixbyite, $Ia3$ containing two sites, 1/4 of symmetry ($\bar{3}$) and 3/4 of symmetry (2)), while at high temperatures the B-phase (crystal class $C2/m$, three different sites of symmetry (m) of equal multitude (1/3)) are formed [1]. The locally sensitive γ-ray perturbed angular correlation method (PAC) is well suited to investigating crystal phases [2] as well as local defects [3] by means of the hyperfine interaction of the specific probe nucleus with its environment. The electric field gradients for ^{111}Cd at defect-free cationic sites have been determined for many classes of binary oxides [2]. In particular, the cubic C-phase of the rare earth sesquioxides has been well investigated with the PAC method [4–6], but only one PAC experiment identifying the monoclinic B-phase is presently known to us [7]. The temperature dependence of the EFG has not been measured in this class of compounds. As the point-charge model (PCM) worked perfectly in the cubic C-phase sesquioxides, it was interesting to see whether this was equally true in the monoclinic B-phase. This phase of the rare earth oxides is formed at high temperatures essentially because of entropy reasons [8], and stays metastable at lower temperatures. It was furthermore interesting to see whether defects exist in this phase and are trapped at the tracer impurities.

Hyperfine parameters have previously been measured via Mössbauer spectroscopy in B-Gd_2O_3 and Eu_2O_3. Barton and Cashion [9] measured the electric field gradients in several ionic compounds of gadolinium including B-Gd_2O_3. Unfortunately the $I = \frac{3}{2}$ level of ^{155}Gd used in their Mössbauer experiment does not allow a separate determination of ν_Q and η. As they used calculated values for η and the principal component of the field gradient V_{zz}

0953-8984/94/4810445+12$19.50

to extract the Sternheimer antishielding factor of the $^{155}Gd^{3+}$ ion, a direct comparison of the experimental ν_Q with those of ^{111}Cd probes is not possible. For different Eu isotopes isomer shifts of Mössbauer experiments in Eu_2O_3 have been reported [10] but no EFG, so a comparison with our experiments was not possible.

2. Sample preparation and PAC measurements

All samples used in our experiments consisted of high-purity oxides (Johnson Matthey Gd_2O_3 99.999%, Sm_2O_3 99.999%, Eu_2O_3 specpure 120 ppm) pressed into pellets under 0.6 kbar. The C → B phase transition of the oxides was achieved by heating the pellets in air at elevated temperatures: Sm_2O_3 for 16 h at 1670 K; Eu_2O_3 for 21 h at 1640 K; Gd_2O_3 for 16 h at 1670 K. About 10^{12} $^{111}In^+$ ions were implanted at 400 keV using the Göttingen ion implanter IONAS.

After the implantation an annealing of 1 h at about 1370 K in air was fully sufficient to remove all radiation damage. In Gd_2O_3 all radiation damage was removed after 1 h of annealing above 1000 K. Afterwards there was no further reduction of linewidth. No sharp EFG except for those seen in the fully annealed samples was obtained at intermediate annealing temperatures or times. A 16 h annealing at 1370 K yielded no further changes.

All temperature-dependent measurements were performed at a pressure of less than 10^{-5} mbar either in a coaxial wire oven (300–900 K) or in a closed-cycle He cryostat (14–290 K). The precision in temperature for the oven was about ±3 K and for the cryostat ±0.5 K.

The PAC data were taken with standard four-detector setups equipped with either NaI or BaF_2 detectors [11, 12].

The PAC method [13, 14] and the interpretation of quadrupole coupling constants in terms of the point-charge model have been well described elsewhere [2]. We thus restrict ourselves here to a short outline of the method. It uses a γ cascade to determine the hyperfine splitting of the intermediate nuclear state of quadrupole moment Q, spin I and lifetime τ. The hyperfine splitting is caused by the interaction of the static EFG tensor V_{ij} with the quadrupole moment Q of the intermediate state. In the case of ^{111}Cd the sensitive level ($I^\pi = 5/2^+$, $Q = 0.83$ b and $\tau = 122$ ns [13]) is populated by a 171 keV γ_1-decay from the $I^\pi = 7/2^+$ state, which itself is fed by $^{111}In(EC)^{111}Cd$ electron capture radioactive decay. For polycrystalline samples the time-differential angular correlation, which means the probability of detecting the second γ-ray γ_2 (248 keV) at an angle Θ relative to the first at time t, is given by

$$W(\Theta, t) = 1 + A_{22}G_{22}(t)P_2(\cos\Theta) \tag{1}$$

where A_{22} denotes the anisotropy coefficient and $P_2(\cos\Theta)$ the second Legendre polynomial; G_{22} contains all information about the hyperfine interaction of the probe ion with its environment.

The traceless EFG tensor V_{ij} is usually represented in its diagonalized form. Two parameters can then describe the EFG, the coupling constant

$$\nu_Q = eQV_{zz}/h \tag{2}$$

and the asymmetry parameter

$$\eta = \frac{V_{xx} - V_{yy}}{V_{zz}} \tag{3}$$

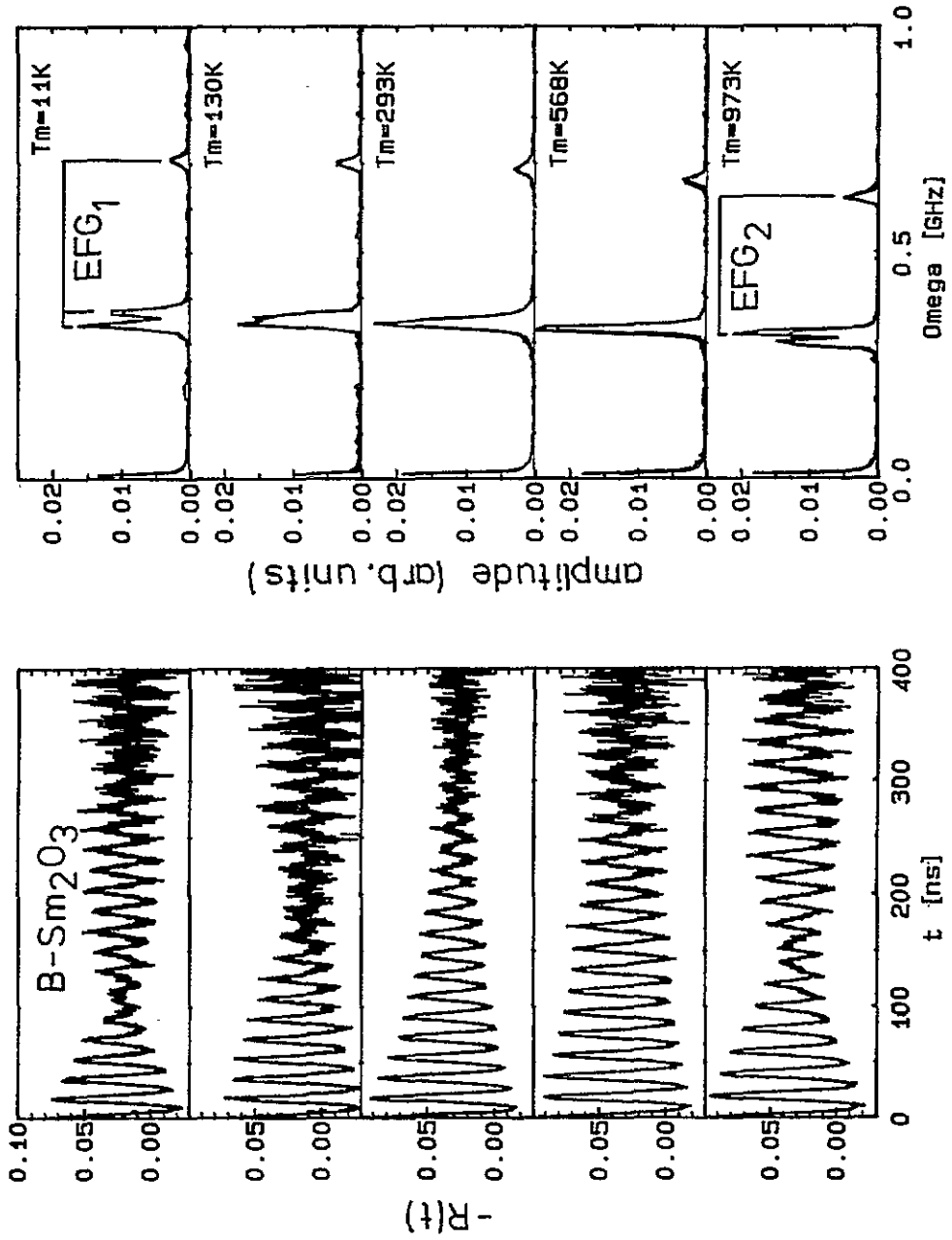

Figure 1. PAC spectra and their Fourier transforms in B-phase Sm_2O_3 at different temperatures. All spectra were taken at $p_m = 10^{-5}$ mbar. Experimental points and fits are plotted for $R(t)$ and its Fourier transform.

with $0 \leqslant \eta \leqslant 1$ and $|V_{xx}| \leqslant |V_{yy}| \leqslant |V_{zz}|$. The coupling constant ν_Q contains information about the strength of the interaction, while the asymmetry parameter indicates the deviation from axial symmetry. For a static electric quadrupole interaction the hyperfine interaction of the probe nucleus generates three frequencies $\omega_n = g_n(\eta)\nu_Q$, giving

$$G_{22}(t) = \sum_{n=0}^{3} s_{2n}(\eta) \cos(\omega_n t) \exp(-g_n(\eta)\delta t). \tag{4}$$

Here $g_n(\eta)$ and $s_{2n}(\eta)$ only depend upon the asymmetry parameter η. A distribution of EFG is described by a Lorentzian frequency distribution of width δ. If several static environments exist the experimental correlation function $R(t)$ is then given by

$$R(t) = A_{22} \sum_i f_i G_{22}^i(t) \tag{5}$$

with f_i being the relative fraction with which each environment contributes to the spectrum.

When calculations of electric field gradients are compared with experimental values, the antishielding of the electron shell of the probe ion has to be taken into account. We used a value of $\beta = -32.9$ [5] to account for the antishielding of the $^{111}Cd^{2+}$ ion.

3. Results

3.1. The dominant EFG$_1$

Figure 1 shows a set of PAC spectra and their Fourier transforms at different measuring temperatures T_m in Sm_2O_3. In all spectra a single EFG_1 of high asymmetry ($\eta \approx 1$) is dominant. Figure 1 clearly shows that the frequencies ω_1 and ω_2 are separated at low temperatures ($\eta = 0.93$), coincide at about 500 K ($\eta = 1$) and are separate again at higher temperatures ($\eta \approx 0.9$). All three sesquioxides in the B phase behave remarkably alike concerning their dominant EFG_1 and its temperature dependence, as shown in figures 1–3. The EFG_1 parameters measured at room temperature are summarized in table 1.

Table 1. Electric field gradients of ^{111}Cd in B-phase rare earth sesquioxides.

		Sm_2O_3		Eu_2O_3		Gd_2O_3	
		ν_Q	η	ν_Q	η	ν_Q	η
EFG_1	(RT)	207.0(3)	0.979(5)	207.6(5)	0.975(8)	208.8(5)	1.00(1)
EFG_2	(773 K)	195(2)	1.00(5)	195.9(5)	1.00(1)	199.0(5)	1.00(2)
EFG_3	(RT)	——	——	217(2)	0.50(2)	221(8)	0.50(1)

The definitions of ν_Q and η yield discontinuities when η reaches the value $\eta = 1$, which means a redefinition of the EFG orientation in the lattice. This effect is clearly visible for the temperature-dependent values of ν_Q and η in Sm_2O_3 displayed in figure 4. To avoid this discontinuity the temperature dependence of the EFG tensor components of the dominating EFG_1 are themselves displayed in figure 5; V_{11} and V_{22} are now strictly linear functions of temperature, whose temperature coefficients are given in table 2.

The crossing of V_{11} and V_{22} where the EFG principal axes change orientation in the crystal ($\eta = 1$) arises at the same temperature ($T_m = 480$ K) in all three oxides. Above 480 K, V_{22} becomes the largest component V_{zz} of the field gradient.

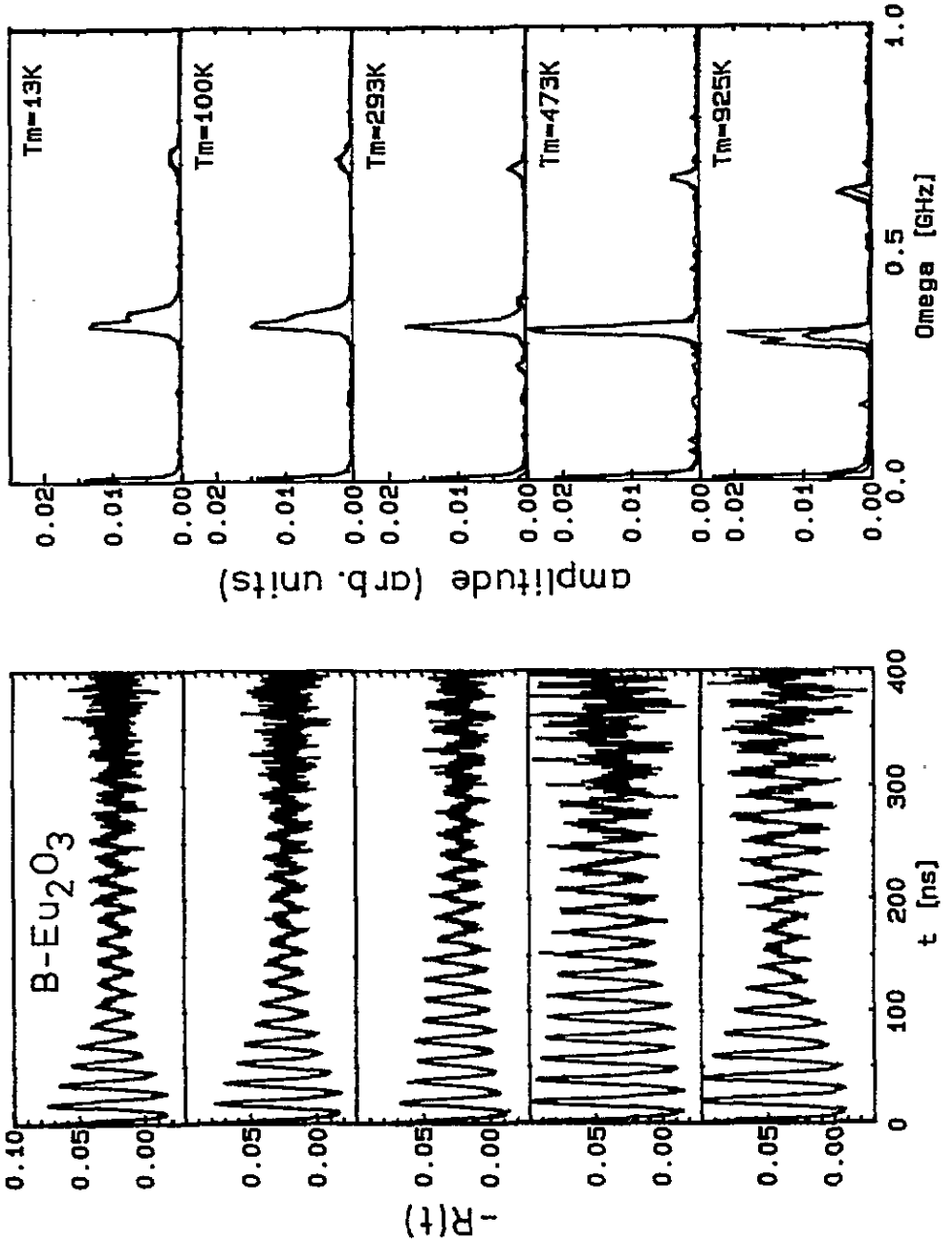

Figure 2. Same as figure 1 for Eu_2O_3.

3.2. Small fractions of EFG$_2$ and EFG$_3$

At some temperatures the spectra cannot be described by the single EFG$_1$ alone. The perturbation function $R(t)$ for a polycrystalline sample demands the amplitude of ω_2 to be lower than for ω_1, as can be seen, for example, in the spectrum of Sm_2O_3 at 11 K (figure 1). In all three oxides a second EFG$_2$ is required to account for the amplitude of ω_2 at high temperatures. In Eu_2O_3 this second EFG$_2$ has to be included at all temperatures to fit the $R(t)$ functions at times $t \geqslant 100$ ns, although it is not immediately visible in all Fourier transforms of figure 2. It is interesting to note that the ν_Q and η values of EFG$_2$ are very close to those of EFG$_1$. For that reason the relative fractions f_1 and f_2 scatter somewhat, while their sum $f_1 + f_2$ can be determined very precisely.

In Gd_2O_3 and Eu_2O_3 a third electric field gradient appears in a small fraction around room temperature. The frequency triplet of this third site can best be seen in the Fourier transform in Gd_2O_3 at room temperature (figure 3). In Eu_2O_3 the fraction of this EFG$_3$ is smaller, but its contribution is still discernible even in the perturbation function $R(t)$. In Sm_2O_3 EFG$_3$ was not found. Figure 6 summarizes the relative fractions of all electric field gradients as a function of temperature T_m.

4. Discussion

4.1. Site occupation

The rare earth sesquioxides crystallize in three isomorphous crystal phases (A,B,C) below about 2300 K. In the hexagonal A-phase [15] as well as in the cubic bixbyite C-phase inequivalent sites of the cations are substituted by the ^{111}In ions according to their statistical weight in the structure. Our results show that in the B phase the three crystal sites (see figure 7) which should have equal multiplicity are at no temperature equally populated by the ^{111}In probes.

In all C-phase sesquioxides, including Sm_2O_3, Eu_2O_3 and Gd_2O_3, the EFG measured with the ^{111}In/^{111}Cd probe can be well reproduced by the point-charge model (PCM) [4]. Even a refinement of the atomic positions to a precision of 0.1–0.3 pm was possible using the measured EFG [5, 6]. A compilation of experimental EFG for substitutional ^{111}In in many binary oxides with ionic binding [2] demonstrated that the PCM reproduces fairly well the symmetry and strength of the EFG as long as the distances between ^{111}Cd and the neighbouring oxygen ions exceed about 210 pm. As can be seen from table 3, this should also be valid for the B-phase sesquioxides.

The values for ν_Q and η calculated at all three substitutional cation sites in the B-phase are listed in table 4.

It can be readily seen that the hyperfine parameters of site M(3) (M = metal) best correspond to the measured EFG$_1$, but cannot be reproduced precisely. A variation of the ionic positional parameters within the errors of the x-ray data yielded the errors of the calculated values [2]. There seems to be no reason why the ionicity in the B phase of the rare earth oxides should be reduced as compared to the C phase. As a consequence, the difference between the calculated values and the measured ones may be due to a slight rearrangement of the direct environment or a slight positional shift of the $^{111}In^{3+}$ ion because of its different ionic size and its preference for a particular geometry of the direct neighbourhood. In ions in C-phase In_2O_3 occupy octahedral sites of perfect ($\bar{3}$) or distorted symmetry (2) [16]. In the B phase all cations are basically coordinated by seven oxygen ions, six of which are fairly close, whereas the seventh oxygen ion (shown hatched in figure 7) is clearly further

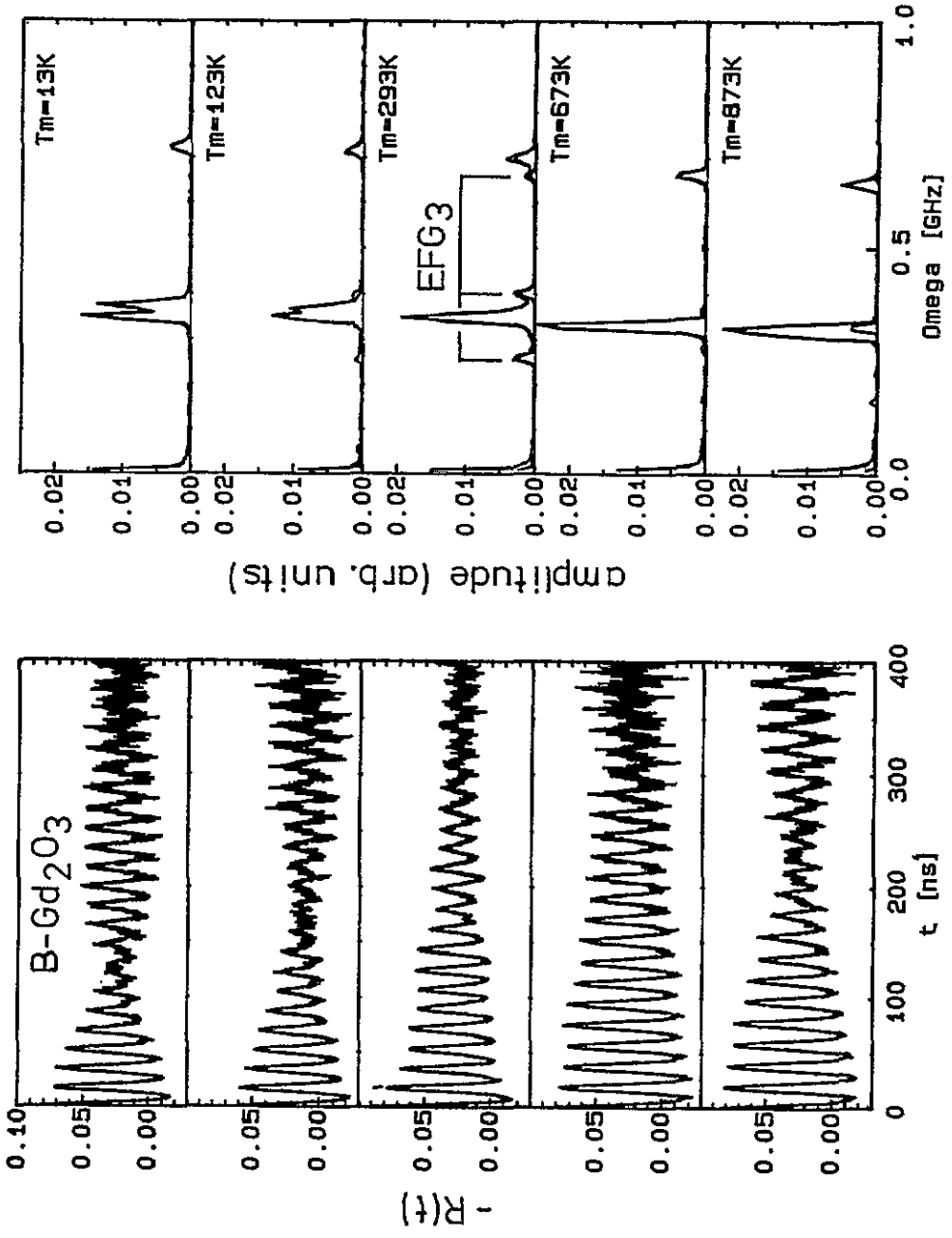

Figure 3. Same as figure 1 for Gd_2O_3.

Table 2. Temperature coefficients of the temperature dependence of the experimental coupling constants of ^{111}Cd in B-phase rare earth sesquioxides: $V_{ii} = V_{ii}\ (T = 0\,\mathrm{K}) - \alpha_{ii} * T$.

	Sm_2O_3	Eu_2O_3	Gd_2O_3
$V_{11}(0)$ [10^{22} V m^{-2}]	1.087(2)	1.097(3)	1.104(2)
α_{11} [10^{18} V m^{-2} K^{-1}]	1.89(7)	2.00(5)	1.85(8)
$V_{22}(0)$ [10^{22} V m^{-2}]	1.046(2)	1.054(3)	1.069(7)
α_{22} [10^{18} V m^{-2} K^{-1}]	0.98(7)	1.07(5)	1.04(8)

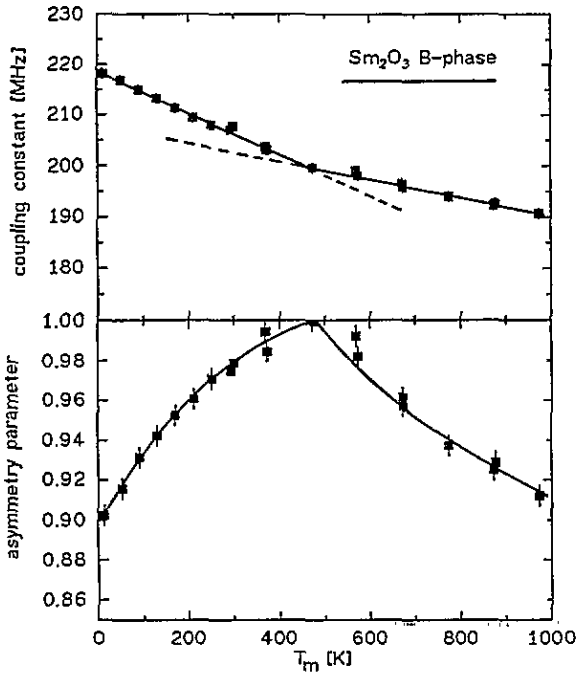

Figure 4. Temperature dependence of the coupling constant ν_{Q1} and asymmetry parameter η_1 of the dominating EFG_1 in B-phase Sm_2O_3.

away, as can be seen in table 3. This particular seventh distance is the largest at site M(3) as compared to site M(1) and M(2). Site M(3) may therefore be better represented by an octahedron, displayed in figure 7. In the plane common to the two pyramids forming the octahedron, the seventh oxygen ion is located at a large distance and hardly contributes to the forces sensed by the $^{111}In^{2+}$ due to the $1/r^2$ dependence of the electric field. Site M(3) best resembles the sixfold coordinated octahedra which In is preferably occupying. The mean distance of M(3) to the six next oxygen neighbours is closest to the average distances in In_2O_3 (218(5) pm [16]).

4.2. Temperature dependence of EFG_1

The coupling constant decreases linearly with temperature. To our knowledge no temperature-dependent structural data exist, a precise comparison of PCM results and measured EFG is not possible, except at room temperature. We tried to estimate the influence of structural changes on the temperature dependence of EFG_1 to be able to differentiate between structural and dynamical effects as were found, for example, in Cr_2O_3 [17].

The only data on a temperature-dependent structural behaviour of the B-phase oxides are linear dilatometric expansion data in Sm_2O_3 [18], Eu_2O_3 [19] and Gd_2O_3 [18, 20]. An

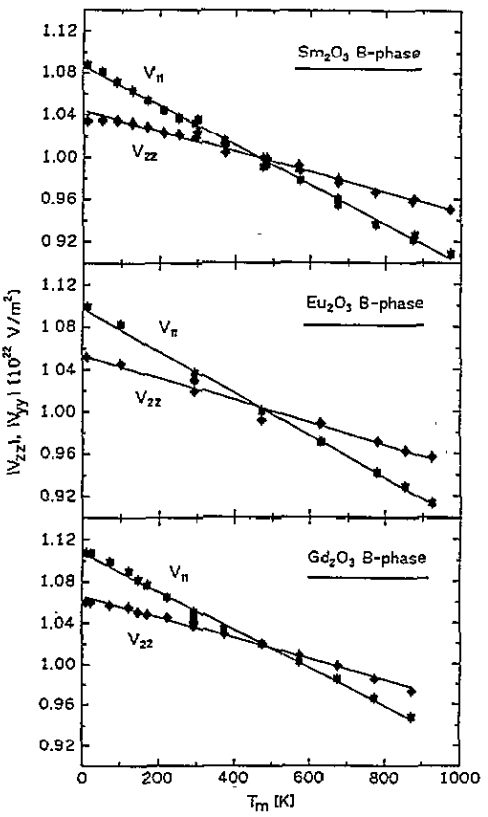

Figure 5. Temperature dependence of the two large components V_{zz}, V_{yy} of the electric field gradient tensor of EFG$_1$ in B-phase rare earth sesquioxides ($V_{xx} = -V_{zz} - V_{yy}$).

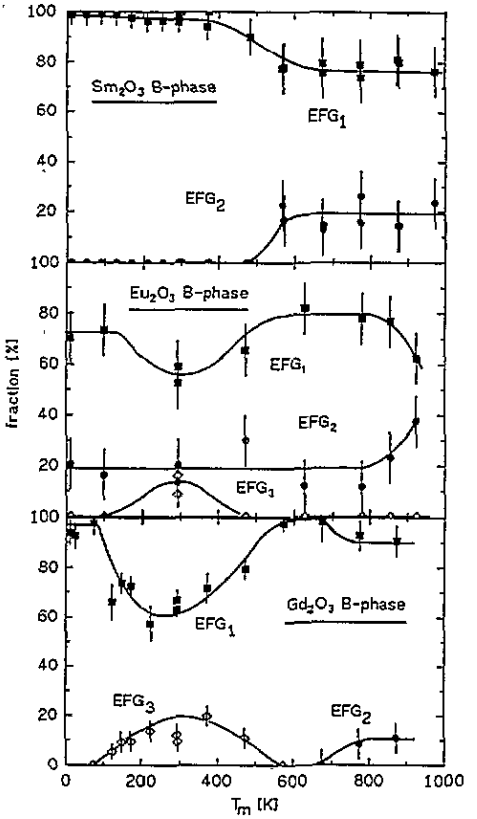

Figure 6. Temperature dependence of the fractions of the three observed EFG to the PAC spectra in B-phase rare earth sesquioxides.

isotropic expansion of the lattice along all three crystal axes yields a calculated reduction in ν_{Q1} of about 3.3(1)% in Sm_2O_3, 2.7(1)% in Eu_2O_3 and 3.5(1)% in Gd_2O_3 between room temperature and 1000 K. This is about half the reduction of the experimental ν_Q by 7.9% in Sm_2O_3, 7.2% in Eu_2O_3 and 8.1% in Gd_2O_3. The asymmetry parameter evidently does not change under the assumed isotropic expansion.

Table 3. Distances (pm) of cations to their nearest oxygen neighbours in B-phase rare earth sesquioxides.

		Site (1)		Site (2)		Site (3)	
		M(1)–O(*i*)	M(1)–O(3)	M(2)–O(*i*)	M(2)–O(5)	M(3)–O(*i*)	M(3)–O(3)
Sm_2O_3	[28]	229.1–254.9	270.1(4)	230.3–248.4	276.1(1)	225.2–256.2	312.3(1)
Eu_2O_3	[29]	229.0–253.7	265.6(4)	228.8–246.2	273.94(2)	223.9–254.4	313.3(4)
Gd_2O_3	[9]	222—252	269(1)	228–245	273(1)	223–253	309(1)

Anisotropic expansion data are only known in B-Gd_2O_3 [20]. The calculations based on these expansion data yielded a slight change of the asymmetry parameter η, but the changes

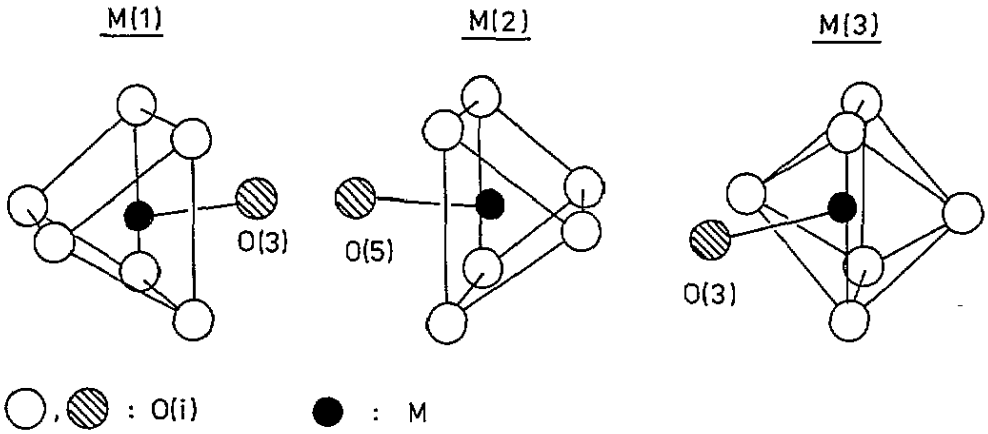

Figure 7. Environments of the three inequivalent cationic sites in B-phase rare earth sesquioxides (from [29]).

Table 4. Calculated electric field gradients with the point-charge model from x-ray coordinates at room temperature ($\beta = -32.95$).

		Site M(1)		Site M(2)		Site M(3)	
		ν_Q (MHz)	η	ν_Q (MHz)	η	ν_Q (MHz)	η
Sm_2O_3	[28]	31(3)	0.06(20)	85(2)	0.42(4)	159(2)	0.82(1)
Eu_2O_3	[29]	24(2)	0.33(10)	88(1)	0.42(3)	162(1)	0.78(1)
Gd_2O_3	[9]	*25(5)*	*0.47(20)*	*87(5)*	*0.54(10)*	*139(9)*	*0.89(5)*

of ν_Q were even smaller than for the isotropic expansion. We also considered anisotropic expansion data from the structurally very similar A-phase oxides La_2O_3 and Nd_2O_3 [21], which can be projected onto the monoclinic cell [22]. This also resulted in too small a frequency shift.

The PAC data thus seem to provide evidence for slight positional changes of the ions within the unit cell with temperature. Whether this change only takes place in the immediate environment of the probe ion, or whether the ions change their positions within the lattice, cannot be decided from the PAC point of view. No definite interpretation is possible without precise temperature-dependent x-ray or neutron diffraction measurements.

4.3. The influence of defects: EFG_2 and EFG_3

EFG_2 and EFG_3 are only observed in very limited temperature ranges where no phase transitions have been observed. Furthermore, their fractions were reversibly reproduced with temperature. As the mobility of ions around room temperature is very low, a population of another crystal site in this temperature range yielding EFG_3 can be excluded. The occupation of another site at high temperatures yielding EFG_2 seems unlikely, because the parameters of EFG_1 and EFG_2 are very similar and very different from those calculated for the other crystal sites. We therefore consider defects to be responsible for EFG_2 and EFG_3.

All three observed EFG show remarkably small distribution widths ($\delta \leqslant 3$ MHz) in all three oxides, which indicates almost perfect environments of the probe ion. This then requires defects to occupy well defined positions in the immediate environment of the probe

ion. Statistically distributed defects in a concentration of 2 at.%, on average, would place one defect in the third-nearest-neighbourhood of the $^{111}In^{3+}$ ion and broaden the spectra. Much lower concentrations of defects may yield different EFG if these defects are trapped by the $^{111}In^{3+}/^{111}Cd^{2+}$ ions. However, the small distribution widths actually observed for all three EFG clearly suggest that the defects responsible for the observed EFG_2 and EFG_3 are located at single, well defined positions in the immediate environment of the probe ion.

4.3.1. EFG_2. In Sm_2O_3 and Gd_2O_3 EFG_2 only appears at high temperatures (600–800 K). This is the range where intrinsic vacancy-type defects are formed in sesquioxides and become mobile. In Sm_2O_3 and Eu_2O_3 the ionic conductivity becomes dominant above 800 K [23]. The observed rise of the fraction of EFG_2 in Sm_2O_3 at 600 K and in Gd_2O_3 at 800 K may therefore be correlated with the onset of ionic conduction at approximately these temperatures. The mobility of oxygen ions in the rare earth oxides is known to be higher than those of the cations. As all measurements were carried out at about 10^{-5} mbar, it is tempting to assume that the observed EFG_2 is caused by a trapped oxygen vacancy. The constant amount of probes experiencing EFG_2 in the PAC spectra of Eu_2O_3 at all temperatures is, however, somewhat puzzling.

4.3.2. EFG_3. This fraction is observed between 200–500 K in Gd_2O_3 and Eu_2O_3. It reaches a maximum of 20% in Gd_2O_3 and 10% in Eu_2O_3 (see figure 6). Trapping of oxygen vacancies at ^{111}Cd, as assumed before for explaining EFG_2, does not seem to be reasonable for EFG_3, because the ionic conductivity below 700 K is smaller and decreases with an activation energy twice as large as the conductivity due to holes. All three oxides are known to be p-type conductors between 500 K (lowest temperature quoted) and 800 K. Hole conductivity in Sm_2O_3 is ten times larger than in Gd_2O_3 and five times larger than in Eu_2O_3, independent of temperature [23, 24]. It is therefore tempting to assume that a hole trapped near the ^{111}Cd impurity generates EFG_3. Evidence for such hole trapping mechanisms has been given for Ga_2O_3 and Cr_2O_3 [17, 25] and will be further pursued in a forthcoming paper on PAC measurements in La_2O_3 [26]. There are two sources of electron holes: those of the bulk connected with the p-type conduction, and holes created during the electron capture process $^{111}In^{3+} \xrightarrow{EC} {}^{111}Cd^{3+} \longrightarrow {}^{111}Cd^{2+} + 1h^{+}$ and perhaps more by Auger processes. These holes are intimately related to the probe nucleus. Therefore, if the p-conductivity were continuously lowered with decreasing temperature, all probe ions should eventually see EFG_3. As this is not the case, clearly visible in figure 6, some change in the conductivity behaviour, for example a change towards n-conductivity, has to occur. As the conduction mechanism in these B-phase oxides below 500 K is unclear we are not in a position to prove this change is due to n-conductivity, but consider it the most probable mechanism to explain the appearance of EFG_3 in Gd_2O_3 and Eu_2O_3.

There was no observable influence of the humidity of the environmental atmospheres on the PAC spectra in Gd_2O_3. As EFG_3 was not observed in Sm_2O_3, along with the fact that the proton solubility in Sm_2O_3 is higher than in Gd_2O_3 [27], the influence of protons does not seem to be important here.

5. Summary

The PAC spectra of ^{111}Cd in the monoclinic B-phase rare earth sesquioxides Sm_2O_3, Eu_2O_3 and Gd_2O_3 display a remarkably similar behaviour. The strongly populated EFG_1 of high asymmetry ($\eta \approx 1$) and small distribution width is attributed to the M(3) cation site. The

change of its asymmetry with temperature can only be explained by positional changes of the ions in the unit cell. The remarkable effect that out of three equivalent ionic sites only one site is substitutionally populated by the ^{111}In probes can be explained by the smaller ionic radius of the In^{3+} ion and its preference for octahedral coordination. The two other EFG observed in small fractions and in limited temperature intervals are probably caused by defects. Around room temperature holes (EFG_3), and at high temperatures oxygen vacancies (EFG_2), are suggested to be trapped by some of the probe ions.

Acknowledgments

The authors are grateful to Dr L Ziegeler and D Purschke for their help during the ^{111}In implantations. This work was supported by the Deutsche Forschungsgemeinschaft.

References

[1] Eyring L 1979 *Handbook on the Physics and Chemistry of the Rare Earths* ed K A Gschneider and L Eyring (Amsterdam: North Holland) p 337
[2] Wiarda D, Uhrmacher M, Bartos A and Lieb K P 1992 *J. Phys.: Condens. Matter* **5** 4111 and references therein
[3] Evenson W E, Gardner J A, Wang R, Su H T and McKale A G 1990 *Hyperfine Interact.* **62** 283
[4] Bartos A, Lieb K P, Pasquevich A F and Uhrmacher M 1991 *Phys. Lett.* **157A** 513
[5] Bartos A, Lieb K P, Uhrmacher M and Wiarda D 1993 *Acta Crystallogr.* B **49** 165
[6] Lupascu D, Bartos A, Lieb K P and Uhrmacher M 1994 *Z. Phys.* B **93** 441
[7] Shitu J, Wiarda D, Wenzel T, Uhrmacher M, Lieb K P, Bedi S and Bartos A 1992 *Phys. Rev.* B **49** 7987
[8] Rudenko V S and Boganov A G 1970 *Inorg. Mater. USSR* **6** 1893
[9] Barton W A and Cashion J D 1979 *J. Phys. C: Solid State Phys.* **12** 2897
[10] *Gmelin Handbook of Inorganic Chemistry* 1974 **39** SE C 1 370
[11] Bartos A, Schemmerling K, Wenzel T and Uhrmacher M 1993 *Nucl. Instrum. Meth.* A **330** 132
[12] Bolse W, Uhrmacher M and Lieb K P 1987 *Phys. Rev.* B **36** 1818
[13] Schatz G and Weidinger A 1992 *Nukleare Festkörperphysik* (Stuttgart: Teubner)
[14] Frauenfelder H, Steffen R M Tolhoek H A de Groot S R and Huiskamp W J 1965 *Alpha-, Beta- and Gamma-ray Spectroscopy* vol 2, ed K Siegbahn (Amsterdam: North Holland) p 997
[15] Lupascu D, Albohn J, Shitu J, Bartos B, Królas K, Uhrmacher M and Lieb K P 1993 *Hyperfine Interact.* **80** 959
[16] Marezio M 1966 *Acta Crystallogr.* **20** 723
[17] Neubauer M, Bartos A, Uhrmacher M, Wenzel T, Lupascu D and Lieb K P 1994 *Europhys. Lett.* submitted
[18] Ploetz G L, Krystyniak C W and Dumas H E 1958 *J. Am. Ceram. Soc.* **41** 551
[19] Preston S D 1980 *High Temp. High Press.* **12** 441
[20] Sawbridge P T and Waterman N A 1968 *J. Mater. Sci.* **3** 15
[21] Taylor D 1984 *Br. Ceram. Trans. J.* **83** 92
[22] Caro P E 1968 *J. Less-Comm. Met.* **16** 367
[23] Subba Rao G V, Ramdas S, Mehrotra P N and Rao C N R 1970 *J. Solid State Chem.* **2** 377
[24] Noddack W and Walch H 1959 *Z. Elektrochem.* **63** 269
[25] Pasquevich A F, Uhrmacher M, Ziegeler L, Lieb K P 1993 *Phys. Rev.* B **48** 10052
[26] Lupascu D *et al* 1994 to be published
[27] Love B 1958 *Gmelin Handbook of Inorganic Chemistry* AD-211847 139 319, 384
[28] Schleid T and Meyer G 1989 *J. Less-Comm. Met.* **149** 73
[29] Yakel H L 1979 *Acta Crystallogr.* B **35** 564